Synthesis of Silicalite Membrane with an Aluminum-Containing Surface for Controlled Modification of Zeolitic Pore Entries for Enhanced Gas Separation

Authors:

Shaowei Yang, Antonios Arvanitis, Zishu Cao, Xinhui Sun, Junhang Dong

Date Submitted: 2018-07-31

Keywords: gas separation, pore modification, zeolite membrane

Abstract:

The separation of small molecule gases by membrane technologies can help performance enhancement and process intensification for emerging advanced fossil energy systems with CO? capture capacity. This paper reports the demonstration of controlled modification of zeolitic channel size for the MFI-type zeolite membranes to enhance the separation of small molecule gases such as O? and N?. Pure-silica MFI-type zeolite membranes were synthesized on porous ?-alumina disc substrates with and without an aluminum-containing thin skin on the outer surface of zeolite membrane. The membranes were subsequently modified by on-stream catalytic cracking deposition (CCD) of molecular silica to reduce the effective openings of the zeolitic channels. Such a pore modification caused the transition of gas permeation from the N?-selective gaseous diffusion mechanism in the pristine membrane to the O?-selective activated diffusion mechanism in the modified membrane. The experimental results indicated that the pore modification could be effectively limited within the aluminum-containing surface of the MFI zeolite membrane to minimize the mass transport resistance for O? permeation while maintaining its selectivity. The implications of pore modification on the size-exclusion-enabled gas selectivity were discussed based on the kinetic molecular theory. In light of the theoretical analysis, experimental investigation was performed to further enhance the membrane separation selectivity by chemical liquid deposition of silica into the undesirable intercrystalline spaces.

Record Type: Published Article

Submitted To: LAPSE (Living Archive for Process Systems Engineering)

Citation (overall record, always the latest version): LAPSE:2018.0303
Citation (this specific file, latest version): LAPSE:2018.0303-1
Citation (this specific file, this version): LAPSE:2018.0303-1v1

DOI of Published Version: https://doi.org/10.3390/pr6020013

processes

MDPI

Article

Synthesis of Silicalite Membrane with an Aluminum-Containing Surface for Controlled Modification of Zeolitic Pore Entries for Enhanced Gas Separation

Shaowei Yang †, Antonios Arvanitis, Zishu Cao, Xinhui Sun and Junhang Dong *

Department Chemical and Environmental Engineering, University of Cincinnati, Cincinnati, OH 45221, USA; shaowei.yang@chbe.gatech.edu (S.Y.); arvanias@mail.uc.edu (A.A.); caozu@mail.uc.edu (Z.C.); sunxh@mail.uc.edu (X.S.)

* Correspondence: junhang.dong@uc.edu

† Current address: Georgia Institute of Technology, Atlanta, GA 30332, USA.

Received: 15 January 2018; Accepted: 31 January 2018; Published: 5 February 2018

Abstract: The separation of small molecule gases by membrane technologies can help performance enhancement and process intensification for emerging advanced fossil energy systems with CO_2 capture capacity. This paper reports the demonstration of controlled modification of zeolitic channel size for the MFI-type zeolite membranes to enhance the separation of small molecule gases such as O_2 and N_2. Pure-silica MFI-type zeolite membranes were synthesized on porous α-alumina disc substrates with and without an aluminum-containing thin skin on the outer surface of zeolite membrane. The membranes were subsequently modified by on-stream catalytic cracking deposition (CCD) of molecular silica to reduce the effective openings of the zeolitic channels. Such a pore modification caused the transition of gas permeation from the N_2-selective gaseous diffusion mechanism in the pristine membrane to the O_2-selective activated diffusion mechanism in the modified membrane. The experimental results indicated that the pore modification could be effectively limited within the aluminum-containing surface of the MFI zeolite membrane to minimize the mass transport resistance for O_2 permeation while maintaining its selectivity. The implications of pore modification on the size-exclusion-enabled gas selectivity were discussed based on the kinetic molecular theory. In light of the theoretical analysis, experimental investigation was performed to further enhance the membrane separation selectivity by chemical liquid deposition of silica into the undesirable intercrystalline spaces.

Keywords: zeolite membrane; pore modification; gas separation

1. Introduction

The energy-efficient membrane gas separation technology can play significant roles in performance enhancement and process intensification for the advanced fossil energy systems with CO_2 capture capacity. For the emerging coal- and natural gas-based IGCC power production with CO_2 capture and sequestration (CCS), cost effective air separation unit (ASU) for the gasifier and H_2/CO_2 separation units for pre-combustion CO_2 capture are critical to commercial success. However, both the O_2 and CO_2 gas separations currently remain challenging that hinders the realization of the IGCC-CCS technology. Traditional industrial O_2 separation by cryogenic distillation or pressure swing adsorption (PSA) is highly energy intensive and involves large capital investment. Membrane separation has shown promises as energy-efficient alternative for O_2 separation in the past few decades [1]. However, because of the very close kinetic diameters (d_k) of the O_2 (d_k = 0.346 nm) and N_2 (d_k = 0.364 nm)

molecules and similarly weak adsorbing behaviors of both gases in common membrane materials, low temperature O_2 separation membranes reported in the literature have been of relatively poor performance with limited selectivity and low permeance. The microporous zeolite membranes, because of their extraordinary stability and molecular sieving effects enabled by their uniform sub-nanometer pore sizes, are promising for separating many small molecule gases. The kinetic molecular theory of gas transport in zeolitic pores suggests that, in order to achieve O_2/N_2 selectivity by non-adsorptive diffusion mechanism, the zeolite pore size must situate in between or very near the kinetic diameters of O_2 and N_2 [2,3]. Therefore, in order to achieve size-selectivity between O_2 and N_2 molecules, the zeolite membranes must possess pore diameter (d_p) very close to the kinetic size of N_2, i.e., <0.4 nm.

Membranes of zeolites with pore openings defined by 8-membered rings are promising candidates for O_2 separation because their d_p are around 0.4 nm. The highly siliceous DDR zeolite (d_p ~0.4 nm) membrane has been reported to exhibit O_2/N_2 permselectivity around 2 but the O_2 permeance was only in the order of 10^{-9}–10^{-8} mol/m^2·s·Pa at 298 K [4–6]. Since O_2 and N_2 are both weakly adsorbing with similarly small adsorption amounts in the DDR zeolite [5], the very low O_2 permeance in the DDR zeolite membrane is a result of the large resistance for O_2 transport in the critically sized zeolitic pores over the entire membrane thickness. The membrane of NaA zeolite (d_p ~0.41 nm) was once reported to have surprisingly high O_2/N_2 separation factor of ~7 and O_2 permeance of 2.6×10^{-7} mol/m^2·s·Pa at room temperature [7]. This performance though was observed under vacuum pressure and its reproducibility is yet to be confirmed. In general, for zeolite membranes of very large aluminum contents, such as the A-type membranes, the gas permeation properties are often severely affected by the presence of trace water vapor due to its extremely ionic and hydrophilic surface [8]. In addition, zeolite membranes of such high-aluminum contents are known to experience gradual degradation when subjected to dehydration in vacuum over extended time [9].

Zeolites with pore openings formed by 10-membered rings have effective d_p of around 0.6 nm, which are much less resistive to small gas transport but become incapable of achieving size-selectivity or molecular sieving effect between the closely sized molecules like O_2, N_2, H_2 and CO_2. However, such relatively large pore size allows for depositing molecular modifiers to the internal pore wall to fine tune the effective channel openings. In the literature, highly siliceous MFI-type zeolite membranes, which have nearly cylindrical zeolitic channels formed by 10-membered rings with a diameter of ~0.56 nm, were successfully modified by depositing mono-silica species on their internal pore surfaces. The effective d_p of the internally modified zeolitic channels was estimated to be around 0.36 nm based on the observation of obvious permeance cut-off effects between H_2 and N_2 or CO_2 [3,10,11]. The modification of the MFI-type zeolite membranes by deposition of mono-silica on the internal pore wall using methyldiethoxysilane (MDES) as precursor was first reported by Masuda et al. [10]. The MDES molecule has a linear geometry with nominal dimension of 0.41 nm × 0.91 nm, which can penetrate into the pristine MFI zeolitic channels of 0.56 nm in diameter. The modification was conducted by pre-loading MDES in the zeolitic channels at low temperature followed by calcination to thermally decompose the MDES molecules and deposit mono-silica inside the zeolite channels [10]. After modification, the H_2/N_2 separation factor increased from 1.5~4.5 to 90~140 at 383 K but the H_2 permeance decreased by an order of magnitude to only 2×10^{-8} mol/m^2·s·Pa. The drastic loss of H_2 permeance was attributed to the deposition of mono-silica over the entire channel length that caused enormous resistance to molecular diffusion. An on-stream catalytic cracking deposition (CCD) method was developed in our lab to avoid excessive silica deposition over the channel length [12]. In the on-stream CCD modification process, the MDES precursor is carried in a feed stream during membrane gas permeation operation at around 450 °C where the CCD process can occur at catalytically active sites such as the alumina tetrahedron sites in channel surface without inducing non-catalytic MDES thermal decomposition [3,13,14]. Thus, in principle, after CCD deposition of silica at a single site, this mono-silica deposit creates a narrow "gate" to prevent MDES molecules from entering the rest of channel length. Consequently, the deposition of mono-silica is effectively limited in a small segment of the zeolitic channel while large part of the channel remains in its original size (~0.56 nm)

for fast diffusion [3,15]. The on-stream CCD method alleviated the mass transport resistance increase while achieving selectivity improvement. However, the supported zeolite membrane had largely random distribution of catalytic sites and the locations of CCD depositions were consequentially uncontrolled along the membrane thickness, which is a multiple of individual crystal size in the film. It is conceivable that when the modified site, which could be thought of as a "gate," locates deep down the channel length, the less permeable molecules will have to back diffuse from the gated point to the feed stream during gas mixture permeation. Such a back-diffusion process would inevitably hinder the permeation of the more permeable component.

Here we report the synthesis and on-stream CCD modification of an MFI-type zeolite membrane, which has a pure-silica (i.e., silicalite) base layer with an outer surface of aluminum-containing framework (i.e., ZSM-5), in attempt to effectively control the pore modification within a small depth near the membrane outer surface. The hypothesis is that such a surface "gated" channel structure can improve the gas permeance by avoiding the back diffusion of the less permeable gases without sacrificing permeation selectivity. The modified MFI-type zeolite membranes are examined by permeation for a number of small molecule gases including O_2 and N_2.

2. Experimental

2.1. Materials and Chemicals

The porous α-alumina disc substrates were made of α-alumina powders with an average diameter of 0.46 μm (SG16, Alcoa, TN, USA). The alumina disc was 2-mm thick and 2.6-cm in diameter with porosity and average pore diameter (d_p) of 27–30% and 0.1 μm, respectively. The edge of the disc was sealed by glass and the active membrane area was ~2.5 cm^2 after excluding the glass sealed edge area. The surface of the disc used for membrane coating was polished by 800 mesh sandpaper and washed and dried in an oven at 313 K for overnight before membrane synthesis. The following chemicals and materials were used in the present work: sodium hydroxide (99.99% trace metal basis, pellet, Sigma-Aldrich, USA), fumed silica (0.007 μm, Aldrich, USA), tetrapropylammonium hydroxide (TPAOH, 1 M, Aldrich, USA), sodium aluminate (anhydrous, Al content as Al_2O_3: 50–56 wt. %, Riedel-de Haën, Germany), HNO_3 solution (1.0 M, Fluka, USA) and methyldiethoxysilane (MDES, 96%, Aldrich, USA). All chemicals were used as received. Gases used for membrane permeation tests included H_2 (99.999%), He (99.999%), N_2 (99.999%), O_2 (99.6%), CO_2 (99.99%), CH_4 (99.999%), i-C_4H_{10} (99.5%) and SF_6 (99%). All gases were obtained from Wright Brothers Inc. (Cincinnati, OH, USA) and used as received.

2.2. Synthesis of MFI Zeolite Membranes

Two kinds of MFI-type zeolite membranes were synthesized by the in situ hydrothermal crystallization method under different conditions. The first was a silicalite membrane without an aluminum-containing zeolite surface and the second was a silicalite membrane with an aluminum-containing MFI-zeolite (ZSM-5) outer surface obtained through a two-stage synthesis procedure.

The silicalite membrane without a ZSM-5 surface was obtained from an alumina-free synthesis precursor, which was prepared by mixing 0.35 g NaOH, 5 g SiO_2 and 25 mL 1 M TPAOH solution under vigorous stirring at 353 K. The TPAOH was used as the structure directing agent (SDA). The synthesis solution was aged for four hours at room temperature and then transferred into the synthesis autoclave where the disc substrate was placed horizontally at the Teflon-lined bottom with the polished side facing upward. About 25 mL of the synthesis solution was poured into the autoclave alone the autoclave wall to immerse the alumina disc. The hydrothermal synthesis was conducted at 453 K for 5 h and then the disc membrane was recovered and washed with DI water until the water pH was close to 7. The cleaned membrane disc was dried in an oven at 313 K and then calcined in air at 773 K for 6 h to remove the SDA from the zeolitic pores. This membrane is denoted as M1Si hereafter.

The membrane with a silicalite base layer and a ZSM-5 outer surface was obtained by a two-stage synthesis procedure where the liquid phase composition was varied for the second stage. A specially designed synthesis autoclave, as schematically shown in Figure 1, was employed for the continuous two-stage synthesis. The zeolite precursor solution and hydrothermal reaction conditions for the first stage of synthesis were identical to those used for synthesizing the M1Si. However, the hydrothermal treatment was not terminated in 5 h; and instead, 1.2 mL of sodium aluminate solution (21 wt. % $NaAlO_2$) was injected into the liquid phase by a high-pressure precision syringe pump (KD Scientific, KDS-410, Holliston, MA, USA) and the hydrothermal treatment continued for another hour at 453 K. The reaction was then terminated and the membrane was recovered. The thus synthesized membrane is denoted as M2Al hereafter. Membrane M2Al underwent the same washing, drying and calcining processes as used for preparation of M1Si.

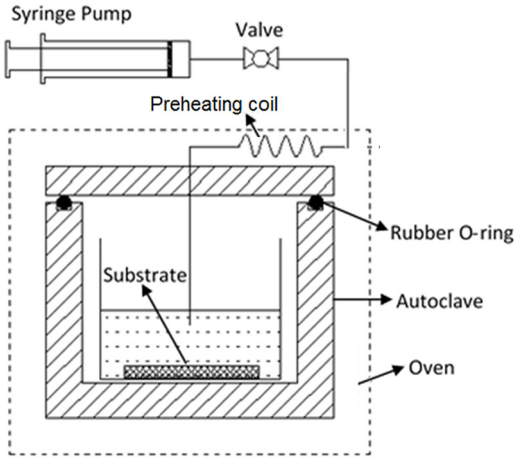

Figure 1. Schematic diagram of the setup used for synthesizing M2Al.

To confirm the formation of a ZSM-5 thin skin on the outer surface of the silicalite crystals by the above described synthesis process, silicalite crystals were synthesized with and without the second stage treatment in $NaAlO_2$ containing solution following the exact procedures used for the syntheses of the two kinds of membranes. The pure-silica MFI-type zeolite (i.e., silicalite) crystals were synthesized using the same aluminum-free precursor and reaction temperature (453 K) and duration (5 h). The thus obtained silicalite particles are denoted as P1Si. In synthesis of the silicalite crystals with a ZSM-5 outer surface, 1.2 mL 21wt. % $NaAlO_2$ solution was introduced into the above silicalite synthesis solution (~25 mL) after 5 h of reaction and the hydrothermal treatment continued for another hour. The thus obtained zeolite particles, which have a ZSM-5 outer surface, are denoted as P2Al.

Both zeolite particulate samples were extensively washed to ensure that any aluminum ions adsorbed on the external surface were completely removed. The washing process including the following consecutive steps: (1) repeated process of zeolite particle dispersion in DI water followed by filtration and rinsing until the filtered water reached pH of ~7; (2) surface cleaning by treating the particles in a 0.1 M NaOH solution under stirring and subsequent ultrasonication for 1 h; (3) washing the NaOH solution-treated zeolite particles by DI water until pH of the washing water reached pH of ~7; (4) treating the cleaned particles in 0.1 M HNO_3 solution under stirring and subsequent ultrasonication for 1 h; and (5) final cleaning by rinsing the zeolite particles with DI water until the filtered water reached pH of ~7. This rigorous surface cleaning process was repeated twice to ensure the complete removal of any aluminum ions and silicate species adsorbed to the external surface of the zeolites. The zeolite particles were then dried and calcined at 450 °C for SDA removal.

2.3. Material Characterizations

The zeolite membranes were examined by X-ray diffraction (XRD, PANalytical, X'Pert Pro MPD, The Netherlands) to confirm the crystal phase and purity. Scanning electron microscopy (SEM, FEI, XL30, Philips, USA) was used to observe the membrane morphology and determine the individual crystallite size and membrane thickness. The energy dispersive X-ray spectroscopy (EDS, EDAX, PV9761/70, NJ, USA) was employed to estimate the elemental compositions at different locations of the zeolite crystals in combination with the transmission electron microscopy (TEM; FEI CM20, Philips, USA).

2.4. Membrane Modification

Figure 2 shows the schematic diagram of the experimental system for CCD modification of the membranes that was essentially the same as that described in our previous publication [12]. This apparatus was also used for membrane gas mixture separation measurements. The disc-shaped zeolite membrane was mounted in a stainless-steel permeation cell using soft graphite gasket seals (Mercer Gasket & Shim, NJ, USA). The membrane permeation cell was placed in a temperature-programmable furnace.

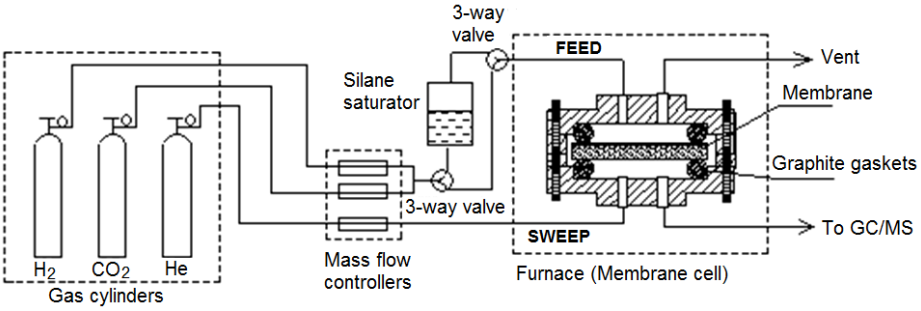

Figure 2. Schematic diagram of the apparatus for membrane modification and gas separation tests.

The CCD modification started with permeation of an equimolar H_2/CO_2 mixture gas fed at a total flow rate of 40 cm^3 (STP)/min when the permeate side was swept by a helium stream at a flow rate of 30 cm^3 (STP)/min. The partial pressure of MDES in the H_2/CO_2 carrier gas was determined to be ~4.3 kPa from the room temperature saturator. The temperature for CCD modification was 723 K at which MDES decomposition occurs catalytically at [AlO_2^-] sites but not on pure silicalite surface, which is noncatalytic. During the gas permeation, the membrane cell was heated up to 723 K at a heating rate of 0.5 K/min and kept at 723 K throughout the modification process. The H_2/CO_2 mixture feed was then switched to bubble through the MDES liquid column to carry MDES vapor before entering the membrane cell. The permeate stream was continuously analyzed by an online gas chromatographer (GC, Agilent 6890N, USA) equipped with a Carboxen 1000 packed column (Supelco, USA) and a thermal conductivity detector (TCD). The H_2/CO_2 separation through the zeolite membrane was continuously monitored during the entire CCD modification process. The feed gas flow was switched back to dry gas feeding route to stop the MDES supply when the online monitored H_2/CO_2 separation factor and gas permeance were stabilized for 2 h.

2.5. Gas Permeation

The membrane was degassed in the permeation cell by vacuuming at 453 K for 12 h prior to testing permeation for each gas. The permeance of pure gases was measured by the transient permeation method in a temperature range from 297 to 773 K with feed pressure of 2 bar using an experimental setup reported a previous publication [16]. The separation of gas mixtures was performed by the conventional steady-state permeation setup (Figure 2) at a feed flow rate of 40 cm^3 (STP)/min and a

helium sweep flow rate of 30 cm^3 (STP)/min. The permeance for gas i ($P_{m,i}$), permselectivity (i.e., ideal selectivity) of gas i over gas j ($\alpha^o_{i/j}$) and separation factor of gas i over gas j in mixture ($\alpha_{i/j}$) are defined as follows:

$$P_{m,i} = \frac{Q}{A_m \cdot t \cdot \Delta P_i} \quad (1)$$

$$\alpha^o_{i,j} = P^o_{m,i} / P^o_{m,j} (i \neq j) \quad (2)$$

$$\alpha_{i/j} = \frac{(y_i / y_j)}{(x_i / x_j)} (i \neq j) \quad (3)$$

where Q (mol) is the moles of gas i permeated through the membrane over a time period of t (s); ΔP_i is the partial pressure difference (i.e., $\Delta P_i = P_{i,f} - P_{i,p}$, where $P_{i,f}$ and $P_{i,p}$ are the partial pressures of gas component i in the feed and permeate sides, respectively); $P^o_{m,i}$ and $P^o_{m,j}$ are pure gas permeance of gas i and gas j, respectively; and x and y are molar compositions of the feed and permeate gas mixtures, respectively.

3. Results and Discussion

3.1. Material Characterizations

The supported zeolite membranes were verified to be of pure MFI-type zeolite phase by the XRD patterns shown in Figure 3. The low intensity of zeolite peaks observed in contrast to the strong peaks of α-alumina substrate was resulted from the thinness of the zeolite layer. Figure 4 shows the SEM images of the two zeolite membranes, i.e., M1Si and M2Al. The zeolite crystals in the two membrane surfaces had very similar shapes of typical siliceous MFI zeolite crystals with individual crystallite size of ~0.3 μm. The SEM pictures of the membrane cross-section also showed zeolite layer thicknesses of ~1 μm for both M1Si and M2Al membranes.

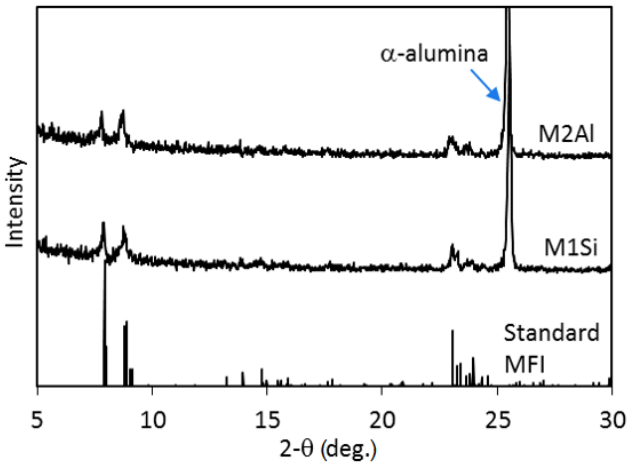

Figure 3. XRD patterns of the MFI membranes M1Si and M2Al together with the standard pattern of silicalite powders [17].

It is well-known that silicalite membranes obtained by in situ crystallization on α-alumina supports in the highly alkaline Al-free precursor used in this work have nearly pure silicalite outer surface but inevitably contain framework aluminum at the zeolite/support interface region [18]. However, because of the thinness of the zeolite layers on the alumina substrates, determining the Si/Al ratios in the zeolite membrane surfaces by EDS elemental analysis is rather challenging. Thus, the incorporation of Al into the framework of silicalite surface was investigated by comparing the two kinds of zeolite particles, i.e., P1Si and P2Al, which were obtained under conditions identical to the syntheses of M1Si and M2Al, respectively. Each zeolite crystal was examined by EDS survey at

two locations, namely the center and corner surfaces of the crystal as shown in Figure 5. The EDS examination used an X-ray beam size of 20 nm in diameter and an operation voltage of 200 kV under which the beam penetration depth was expected to well exceed the zeolite crystal thickness, which was around 200 nm. Crystal P1Si had no detectable Al content (i.e., Si/Al $\rightarrow \infty$) at both locations because no alumina source existed in the precursor throughout the synthesis process. The crystal P2Al had Si/Al ratios of 150 $\pm$ 18 at the center surface and 40 $\pm$ 15 at the corner that confirmed Al incorporation into the framework of zeolite surface. The measured Si/Al ratio was much lower at the corner than at the center because the X-ray beam sampled more surface materials from the side surfaces at the corner than did from the top surface at the center. Since the EDS results are averaged over the depth penetrated by the interrogating X-ray, the Si/Al ratio in the P2Al outer surface must be <40.

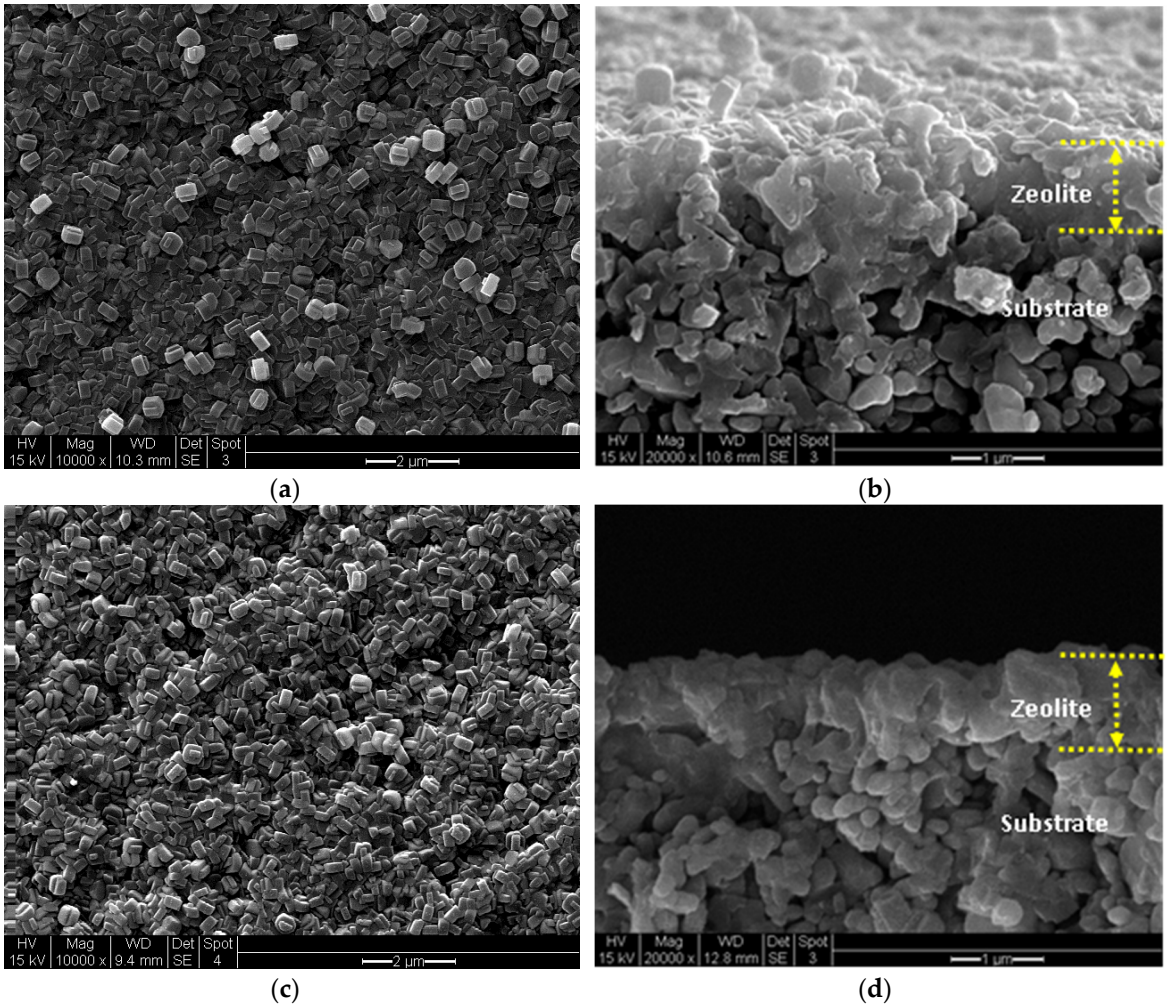

Figure 4. SEM pictures of M1Si and M2Al: (**a**) surface of M1Si and (**b**) cross-section of M1Si; (**c**) surface of M2Al and (**d**) cross-section of M2Al.

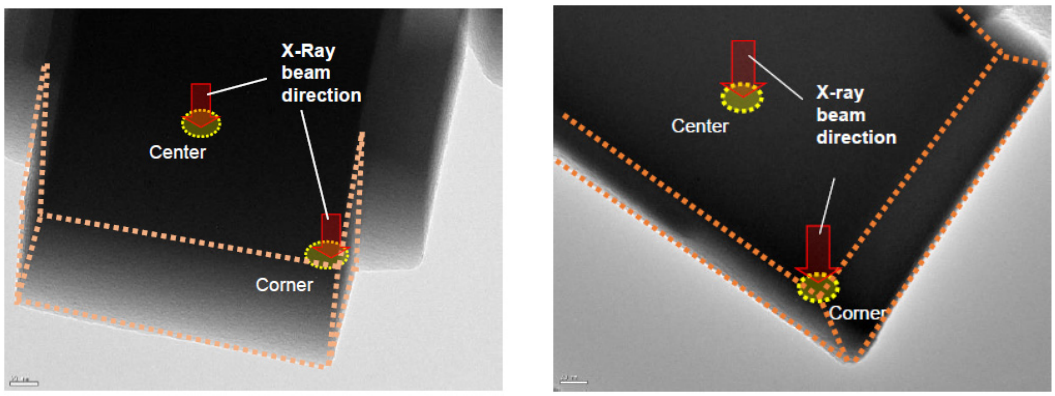

(**a**) (**b**)

Figure 5. TEM pictures and illustration of EDS sampling locations for elemental analyses for the zeolite crystals: (**a**) P1Si and (**b**) P2Al.

3.2. Membrane Modification

The two membranes, i.e., M1Si and M2Al, had similar H_2/CO_2 gas permeation properties before modification that made the modification and subsequent performance analyses and comparisons meaningful. Figure 6 presents the evolution of H_2/CO_2 separation performance for membranes M1Si and M2Al during the CCD modification process. Both fresh membranes exhibited H_2/CO_2 separation factors ($\alpha_{H2/CO2}$) of ~0.2 at room temperature because at room temperature CO_2 is preferentially adsorbed into and diffusing through the zeolitic pores to hinder the entry and permeation of the non-adsorbing H_2 that results in CO_2-selective permeation. The integrity of the membranes was also evidenced by their high permselectivity of H_2 over SF_6 (d_k ~0.55 nm) ($\alpha^o_{H2/SF6,K}$) prior to CCD modification, which was 159 for M1Si and 120 for M2Al at 453 K. The $\alpha_{H2/CO2}$ changed to 2.9 and 2.8 (H_2-selective) for M1Si and M2Al, respectively, when temperature increased to 723 K where adsorption of CO_2 becomes negligible and transport of both CO_2 and H_2 is governed by gaseous diffusion mechanism, which is selective towards the lighter H_2 [3,12]. However, these $\alpha_{H2/CO2}$ values are below the theoretical value ($\alpha_{H2/CO2} = \sqrt{M_{w,CO2}/M_{w/H2}}$) of ~4.69 given by the gaseous diffusion mechanism that indicates enlargement of intercrystalline spaces at high temperature because of the mismatch of thermal expansion coefficient between the zeolite layer and the alumina substrate [19].

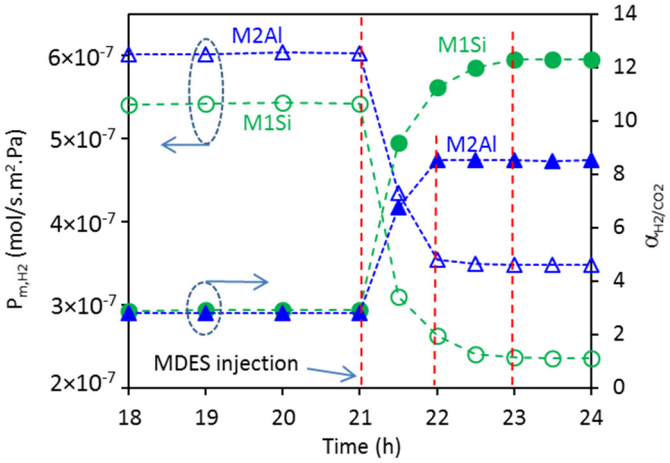

Figure 6. Evolution of the H_2/CO_2 separation factor and H_2 permeance for the two membranes during the CCD modification process.

As shown in Figure 6, after introducing the MDES vapor at 723 K, the permeance of H_2 and CO_2 decreased sharply from 5.42×10^{-7} and 1.87×10^{-7} mol/m^2·s·Pa to 2.36×10^{-7} and 1.92×10^{-8} mol/m^2·s·Pa, respectively, in 2 h for membrane M1Si; and from 6.03×10^{-7} and 2.16×10^{-7} mol/m^2·s·Pa to 3.48×10^{-7} and 4.08×10^{-8} mol/m^2·s·Pa, respectively, in 1 h for membrane M2Al. Meanwhile, $\alpha_{H2/CO2}$ of M1Si and M2Al increased from 2.9 and 2.8 before modification to 12.3 and 8.5 after modification, respectively. The time needed for stabilizing $\alpha_{H2/CO2}$ and H_2 permeance after introducing MDES vapor was noticeably shorter for M2Al (~1.0 h) than for M1Si (~2 h) that might be explained by the different locations of CCD modification in the two membranes. The CCD deposition of mono-silica in the zeolitic channels of M2Al membrane presumably occurred at the outer surface that is expected to complete quickly and essentially no further CCD modification could happen in deeper locations down the zeolite channels because the pore entries are narrowed and become inaccessible to the MDES. On the contrary, the M1Si membrane, are known to have a silicalite outer surface but the framework near the zeolite/alumina-substrate interface contains certain amount of Al^{3+} [12,18]. Thus, the CCD modification in the M1Si membrane takes place deep along the thickness in the channels (close to the zeolite/substrate interface) and thus requires longer time due to the difficult diffusion of MDES molecules and debris of catalytic cracking. The modified M1Si and M2Al are denoted as M-M1Si and M-M2Al, respectively, hereafter. The effective control of pore modification within the surface of M2Al has led to its much higher H_2 permeance ($P_{m,H2}$ ~3.46×10^{-7} mol/m^2·s·Pa) than that of the M-M1Si ($P_{m,H2}$ ~2.36×10^{-7} mol/m^2·s·Pa). However, the M-M2Al exhibited an $\alpha_{H2/CO2}$ of ~8.5 which is lower than that of the M-M1Si ($\alpha_{H2/CO2}$ ~12.3), suggesting that more intercrystalline pores exited in M-M2Al, which could also contribute to its high $P_{m,H2}$.

3.3. Single Gas Permeation for O_2 and N_2

The O_2 and N_2 Single gas permeation was performed as a function of temperature for both membranes before and after the CCD modification. The results are presented in Figures 7 and 8. Before modification, M1Si had O_2/N_2 permselectivity ($\alpha^o_{O2/N2}$) of ~0.925–0.970, which was very close to the Knudsen factor ($\alpha^o_{O2/N2,K}$ ~0.935) for gaseous diffusion, while M2Al had $\alpha^o_{O2/N2}$ of ~0.996–1.03, which was slightly greater than the $\alpha^o_{O2/N2,K}$ in the temperature range of 297–773 K. Since the d_k of O_2 (~0.346 nm) and N_2 (0.364 nm) are significantly smaller than the diameter of the pristine MFI zeolitic pores (d_p ~0.56 nm). The $\alpha^o_{O2/N2}$ was slightly larger than the $\alpha^o_{O2/N2,K}$ because both O_2 and N_2 are weakly adsorbing in the MFI-type zeolites with O_2 having slightly higher adsorption amount [20]. The M2Al exhibited slightly higher $\alpha^o_{O2/N2}$ than M1Si that may be attributed to the higher content of extra-framework Na^+ in the former, which enhances the O_2 adsorption. In addition, the extra-framework metal ions can slightly reduce the zeolitic pore size to favor the diffusion of the smaller O_2. Observations of O_2/N_2 permselectivity greater than Knudsen factor on the alumina supported ZSM-5 membranes have been previously reported in the literature ($\alpha^o_{O2/N2}$ ~1.02–1.16) [21]. The permeance of both O_2 and N_2 exhibited "S"-shaped temperature-dependences on both M1Si and M2Al as shown in Figures 7a and 8a, respectively. As temperature increases, the permeances of O_2 and N_2 increase first and then decrease after passing maxima; as temperature further increases, the permeances increase again after passing minima. Such a temperature-dependence of the permeance ($P^o_{m,i}$) is a result of the adsorption-diffusion transport mechanism because increasing temperature reduces adsorption but enhances the transport diffusivity [22]. The $\alpha^o_{O2/N2}$ values of both unmodified membranes were almost unchanged over the entire temperature range as expected.

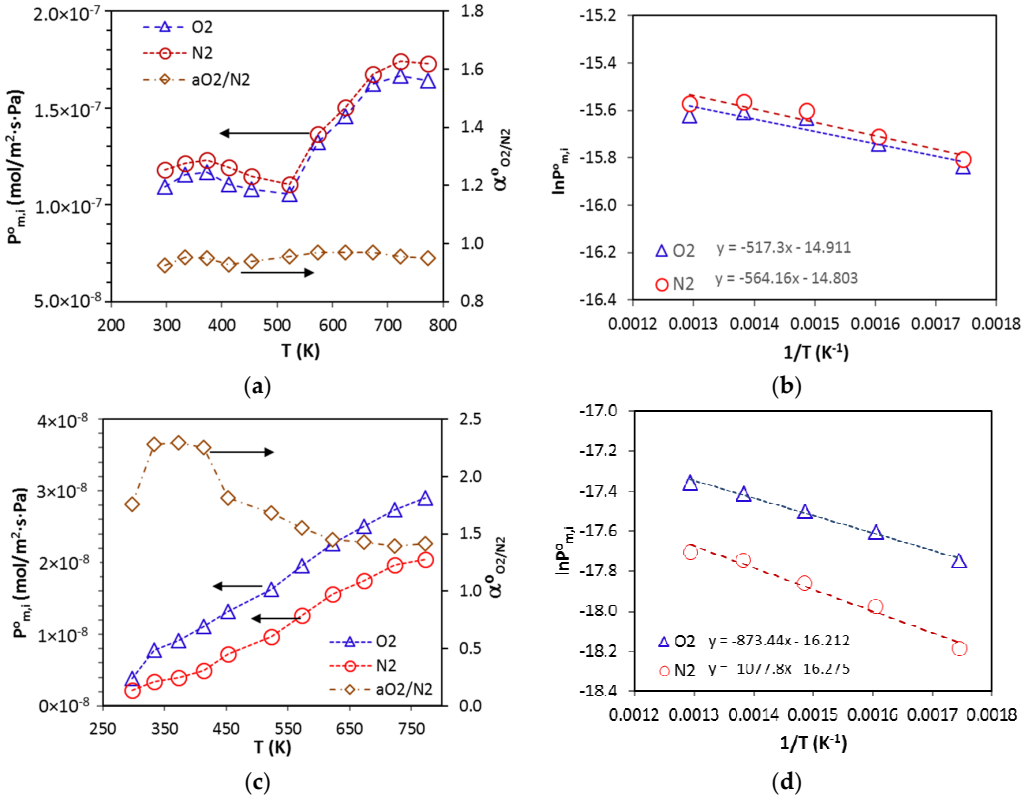

Figure 7. O_2 and N_2 single gas permeation on M1Si and M-M1Si. (**a**,**b**) M1Si and (**c**,**d**) M-M1Si.

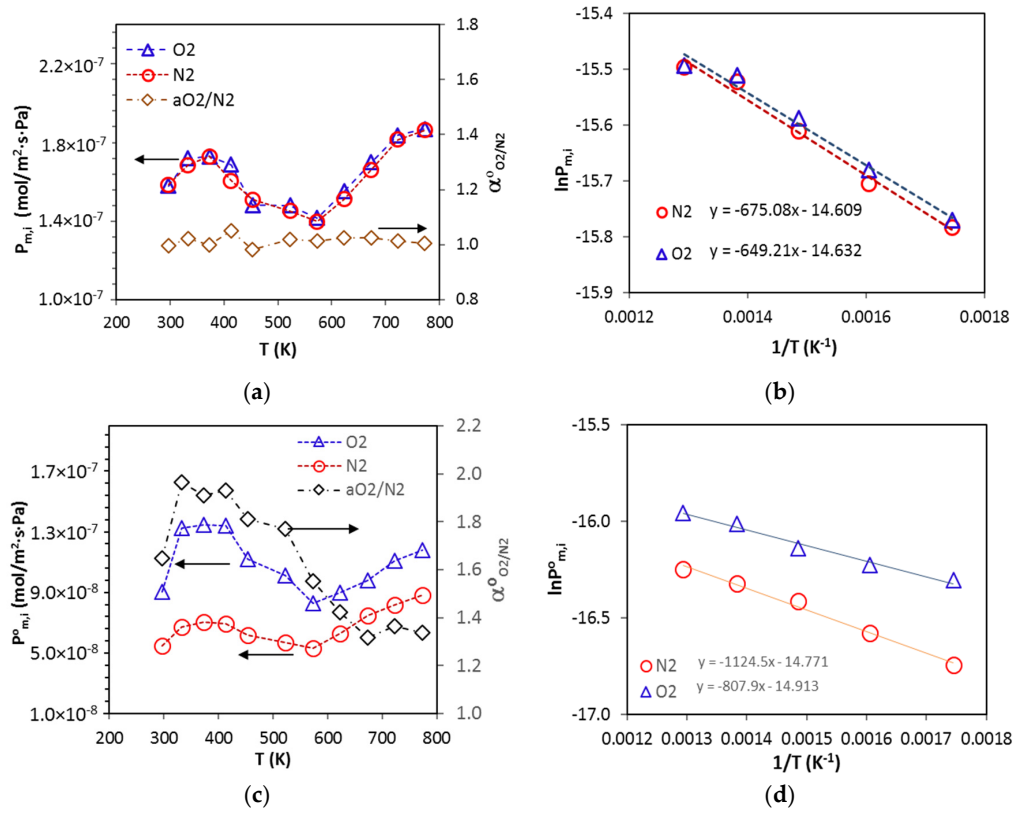

Figure 8. O_2 and N_2 single gas permeation on M2Al and M-M2Al. (**a**,**b**) M2Al and (**c**,**d**) M-M2Al.

In Figures 7b and 8b, the gas permeance of the two unmodified membranes are presented by the Arrhenius plots in the temperature range of 573–773 K, where the adsorption of O_2 and N_2 become negligible. The activation energies ($E_{d,i}$) for diffusion of O_2 and N_2 were similar in the two unmodified membranes, i.e., $E_{d,O2}$ = 4.30 kJ/mol and $E_{d,N2}$ = 4.69 kJ/mol in M1Si; and $E_{d,O2}$ = 5.40 kJ/mol and $E_{d,N2}$ = 5.61 kJ/mol in M2Al. However, the $E_{d,O2}$ and $E_{d,N2}$ are slightly greater in M2Al than in M1Si that again suggest variation of zeolitic channel size due to the difference in amount of extra-framework metal ions between the two membranes.

The gas permeation behavior of the two modified membranes became qualitatively different from their unmodified counter parties. As shown in Figures 7c and 8c, the M-M1Si and M-M2Al were found to be O_2 selective over N_2 with $\alpha^o_{O2/N2}$ much higher than that of the M1Si and M2Al and the selectivity values are opposite to the N_2-selective Knudsen factor for gaseous diffusion mechanism. These indicate that the zeolite channel openings have been effectively narrowed to enable size-selectivity between O_2 and N_2. For the modified membranes, the diffusion activation energy $E_{d,O2}$ and $E_{d,N2}$ were also significantly increased from the values of the unmodified membranes as can be seen in Figures 7d and 8d. The $E_{d,O2}$ and $E_{d,N2}$ were 7.26 kJ/mol and 8.96 kJ/mol, respectively, for M-M1Si; and were 6.72 kJ/mol and 9.35 kJ/mol, respectively, for M-M2Al. Apparently, the CCD modification caused larger increase in $E_{d,N2}$ than $E_{d,O2}$ because N_2 is bigger in size than O_2. In other words, O_2 and N_2 and permeation through the two membranes were governed by gaseous diffusion mechanism before modification, which is selective towards N_2 of smaller mass and became controlled by the activated diffusion mechanism after pore size reduction by the modification, which is selective towards O_2 of smaller size. Interestingly, the temperature-dependences of gas permeance were quite different between the two membranes as shown in Figures 7c and 8c. The M-M1Si exhibited monotonic increase of permeance with increasing temperature that deviates from the "S"-shaped dependence observed before modification. However, the M-M2Al maintained "S"-shaped permeance dependence on temperature, which is similar to that observed on the unmodified membrane. This difference may be caused by the different locations of pore narrowing in the channels of the two modified membranes. In M-M1Si, because the modification presumably occurs near the exiting end of channel and thereby the gas permeation is less influenced by the adsorbing effect since the transport is mainly controlled by the section of reduced channel size.

3.4. O_2/N_2 Mixture Separation

The two modified membranes were also examined for separation of O_2/N_2 mixtures. Figure 9 shows the temperature and pressure dependencies of gas permeance ($P_{m,i}$; i= O_2 and N_2) and separation factor ($\alpha_{O2/N2}$) on M-M1Si for an O_2/N_2 mixture feed with 20/80 molar ratio. It was found that, as feed pressure increased, the $P_{m,O2}$ remained almost unchanged at temperature of 297 K but showed moderate deceases at temperatures of $\geq$333 K; the $P_{m,N2}$, on the other hand, increased slightly as feed pressure increased at 297 K but also decreased moderately at $\geq$333 K. Overall, $P_{m,O2}$ decreased with pressure more rapidly than did $P_{m,N2}$, resulting in decline of $\alpha_{O2/N2}$ with increasing feed pressure. Similar pressure-dependences of gas permeance and $\alpha_{O2/N2}$ were observed for M-M2Al. The decrease in $\alpha_{O2/N2}$ with increasing feed pressure may be explained by considering the increasing contribution of N_2-selective gaseous diffusion through the intercrystalline pores while the transport through the zeolitic pores is less sensitive to pressure as limited by the weak adsorption at zeolite surface. Both $P_{m,O2}$ and $P_{m,N2}$ of the M-M1Si were found to increase monotonically with temperature for all feed pressures due to the activated diffusion mechanism for both gases in the modified membranes. However, due to the difference in magnitude of the temperature dependencies between $P_{m,O2}$ and $P_{m,N2}$, the $\alpha_{O2/N2}$ exhibited bell-shaped temperate-dependence as shown in Figure 9f. The maximum $\alpha_{O2/N2}$ appeared at 373 K for all feed pressures and achieved the best value of ~2.25 with a $P_{m,O2}$ of 7.24×10^{-9} mol/m^2·s·Pa at feed pressure of 1 bar. Thus, for M-M1Si, the gas mixture separation factor $\alpha_{O2/N2}$ was very close to the permselectivity $\alpha^o_{O2/N2}$ (~2.29) but $P_{m,O2}$ was notably lower than the $P^o_{m,O2}$ (9.10×10^{-9} mol/m^2·s·Pa).

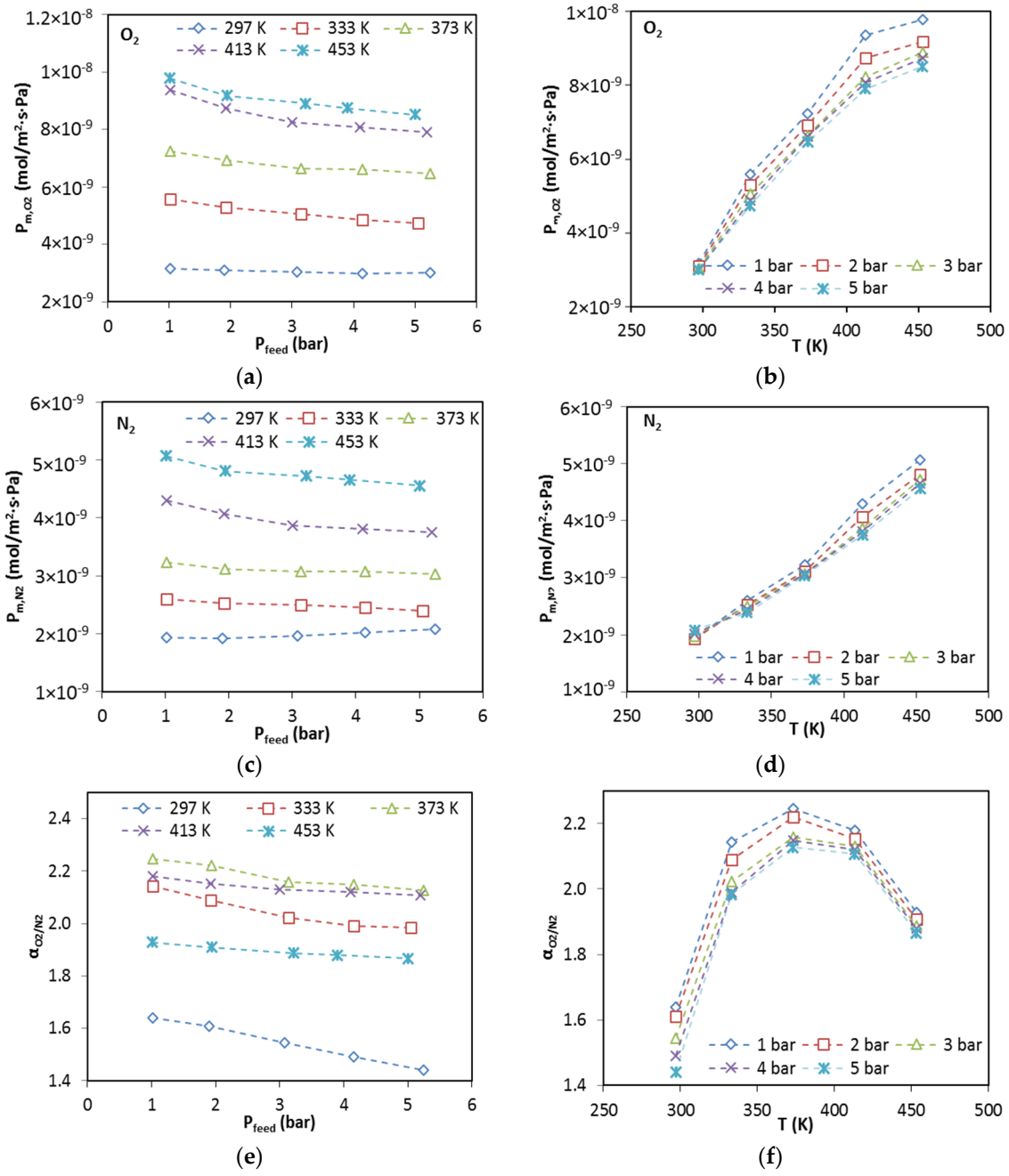

Figure 9. Effects of feed pressure and operating temperature on gas permeance and O_2/N_2 separation factor in the M-M1Si for an O_2/N_2 mixture feed containing 20 mol% O_2. (**a**) $P_{m,O2}$ as a function of pressure; (**b**) $P_{m,O2}$ as a function of temperature; (**c**) $P_{m,N2}$ as a function of pressure; (**d**) $P_{m,N2}$ as a function of temperature; (**e**) $\alpha_{O2/N2}$ as a function of pressure; and (**f**) $\alpha_{O2/N2}$ as a function of temperature.

The results of separation for the 20/80 O_2/N_2 mixture on the M-M2Al membrane are presented in Figure 10. Both $P_{m,O2}$ and $P_{m,N2}$ deceased with feed pressure at all temperatures tested while both $P_{m,O2}$ and $P_{m,N2}$ exhibited bell-shaped dependencies on temperature at each pressure, i.e., increased first and then decreased after reaching maxima at around 333 K. The temperature-dependence of gas permeance on the M-M2Al was again different from that on M-M1Si, which was similar to that observed in single gas permeation. The $\alpha_{O2/N2}$ also exhibited a bell-shaped profile of temperate

dependence at each feed pressure as shown in Figure 10f. The $\alpha_{O2/N2}$ achieved maxima at 333 K, which was lower than the temperature (373 K) for maximum $\alpha_{O2/N2}$ on the M-M1Si. At feed pressure of 1 bar, M-M2Al obtained the best $\alpha_{O2/N2}$ of 1.95, which was almost identical to the $\alpha^{o}_{O2/N2}$ (~1.96) and a $P_{m,O2}$ of 1.2 × 10^{-7} mol/m^2·s·Pa, which was also very close to its $P^{o}_{m,O2}$ (1.3 × 10^{-7} mol/m^2·s·Pa) and far greater than that of the M-M1Si.

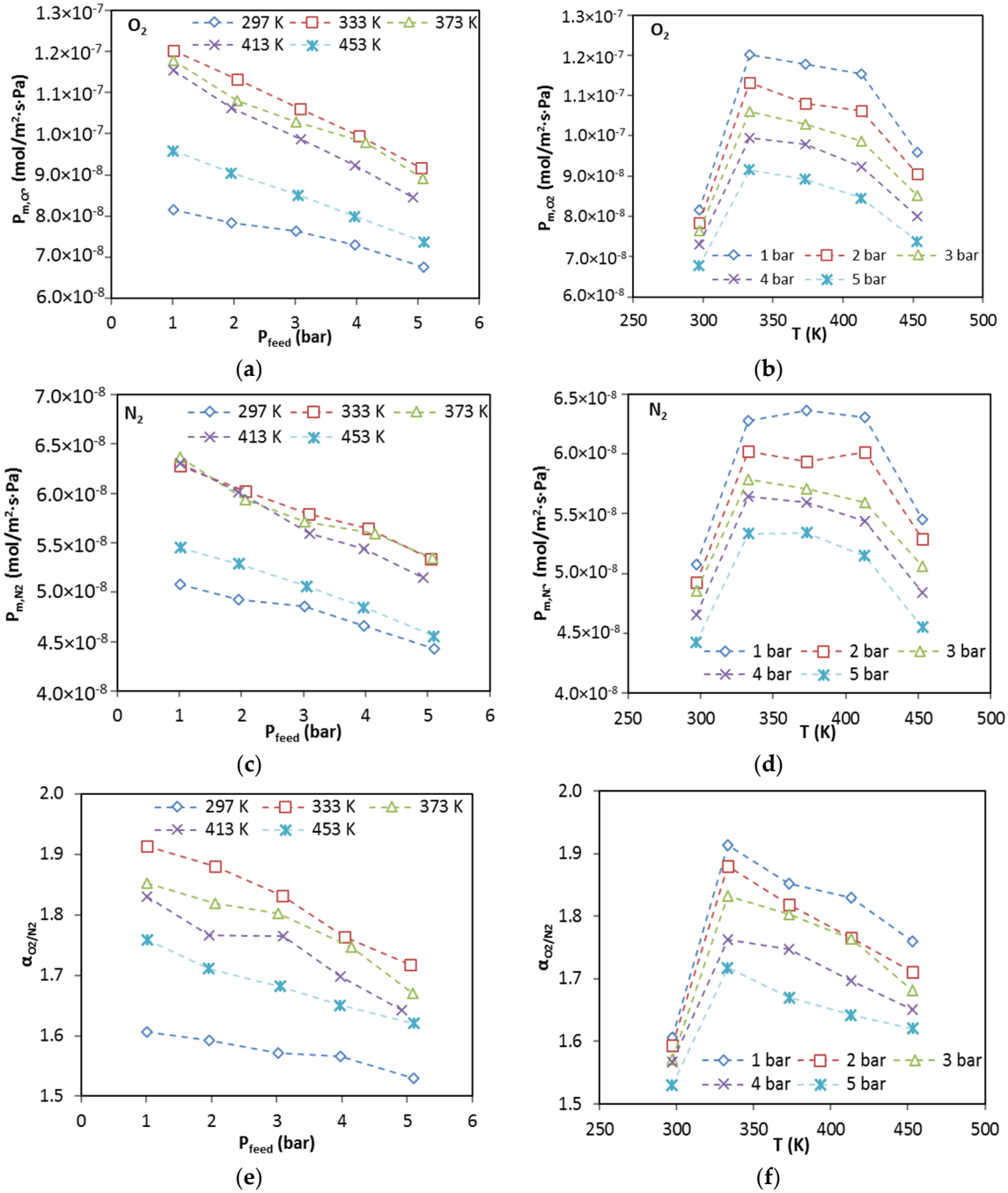

Figure 10. Effects of feed pressure and operating temperature on gas permeance and O_2/N_2 separation factor in M-M2Al for O_2/N_2 mixture feed with 20 mol% O_2: (**a**) $P_{m,O2}$ as a function of pressure; (**b**) $P_{m,O2}$ as a function of temperature; (**c**) $P_{m,N2}$ as a function of pressure; (**d**) $P_{m,N2}$ as a function of temperature; (**e**) $\alpha_{O2/N2}$ as a function of pressure; (**f**) $\alpha_{O2/N2}$ as a function of temperature.

As presented above, in separation of the O_2/N_2 mixture, both M-M1Si and M-M2Al had $\alpha_{O2/N2}$ values very close to their respective $\alpha^o_{O2/N2}$ that was expected from a selectivity largely determined by size exclusion or steric effects at the reduced pore openings. However, $P_{m,O2}$ in mixture permeation was significantly lower than the $P^o_{m,i}$ for M-M1Si while $P_{m,O2}$ remained similar to the $P^o_{m,i}$ for M-M2Al. Such a difference in permeance change between single gas and mixture permeation for M-M1Si and M-M2Al may be caused by the variation of the modification locations along the zeolite channel and membrane thickness as schematically illustrated in Figure 11. The deposition of silica modifier was near the zeolite/substrate interface in M-M1Si but was at the outer surface in M-M2Al. Thus, for gas mixture feed, the O_2 permeation rate is expected to remain very similar to that of single gas permeation in M-M2Al as depicted in Figure 11c but to be inevitably hindered by the back diffusion of the less permeable N_2 from the narrowed section in M-M1Si as depicted by Figure 11b.

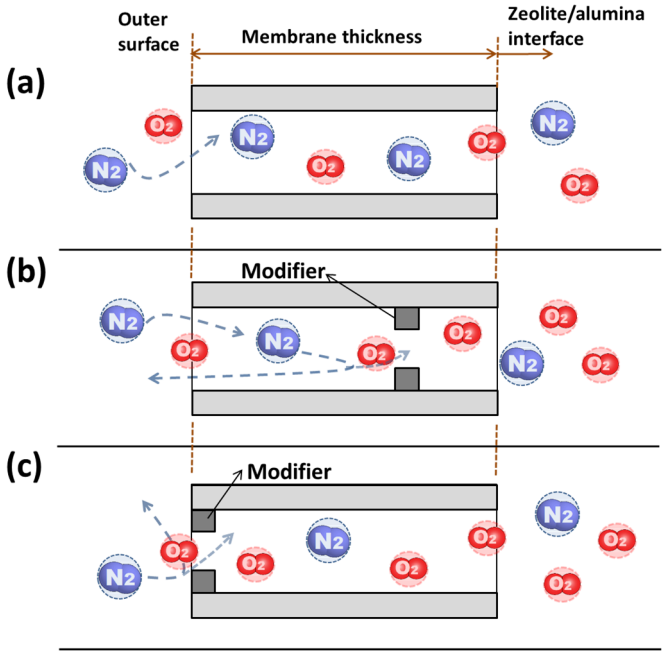

Figure 11. Schematic illustration of the presumed channel structures in the MFI-type zeolite membranes. (**a**) Unmodified; (**b**) M-M1Si; and (**c**) M-M2Al.

3.5. Gas Permeation Selectivity by Size Exclusion

Both M-M1Si and M-M2Al membranes were able to achieve O_2 permselectivity over N_2; however, the M-M2Al with a ZSM-5 surface drastically improved the O_2 permeance as compared to M-M1Si. However, the $\alpha_{O2/N2}$ for both membranes were limited to around 2. The relatively low $\alpha_{O2/N2}$ was attributed primarily to the intercrystalline spaces, which are known to be of nanometer sizes and selective towards the permeation of the lighter N_2. In literature, the effect of pore narrowing in MFI-type zeolite membranes by CCD modification on small gas permeation has been discussed based on the molecular transport model developed by Xiao and Wei [2,3,23]. In the kinetic molecular transport model, gas permeance (P_m) is expressed by Equation (4),

$$P_m = \frac{\varphi}{\delta}(D_o\beta) = \frac{\varphi}{\delta}\cdot\frac{\alpha}{z}\left(\frac{8RT}{\pi M_w}\right)^{1/2}\cdot\beta\cdot\exp\left(-\frac{E_d}{RT}\right) \quad (4)$$

where D_o is jump diffusivity, which correlates with the transport diffusivity D_c and molecule load q in zeolite, i.e., $D_o = D_c/q$ [24]. Under conditions where ideal gas behavior can be assumed and gas adsorption is negligible, q may be represented by $q = \beta P$ [23,25]. φ is a constant depending on the

porosity and tortuosity; δ is the membrane thickness; and α and z are the single jump distance and diffusion coordination number, respectively.

Equation (4) can be used to understand the diffusion mechanisms inside the zeolitic channels according to the magnitude of diffusion activation energy (E_d) obtained from the Arrhenius representation of permeance but cannot correlate the gas selectivity with the size contrast between the molecule and pore opening, i.e., d_k/d_p (=λ), since neither λ nor d_k and d_p is explicitly related in Equation (4). The selectivity for permeating molecules by size discrimination at the channel entrance may be qualitatively analyzed based on kinetic molecular theory and an assumption of elastic collision of hard sphere molecule at pore mouth. At a specific temperature and pressure, the frequency of molecule colliding to the area of channel opening is given the product of gas phase molecular density ($\rho = p/RT$) and molecule travel velocity (υ), which is related inversely to the square root of molecular weight ($\upsilon \propto M^{-0.5}$). As schematically illustrated in Figure 12, when $r_k < r_p$, collisions that can lead to effective entry of molecules must occur within the center area of channel opening defined by r_e (=$r_p - r_k$).

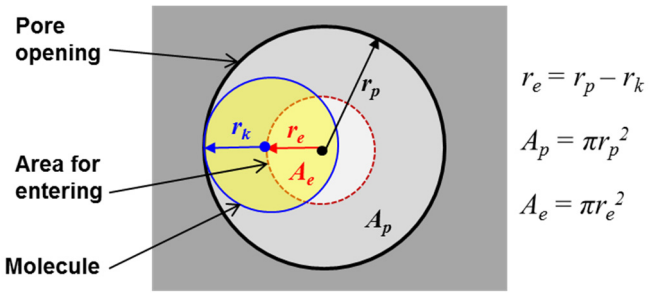

Figure 12. Schematic illustration of molecule entering the zeolite channel entrance.

Therefore, using the original pore radius (r_p = 0.56 nm for MFI zeolite) as the basis of consideration, for molecule "i" with $r_k < r_p$, when permeance is limited by the rate of molecule entering the entrance, $P_{m,i}$ depends on the collision frequency in the entire original pore area A_p (= πr_p^2) and probability (ς) of effective collision in A_e, i.e., $\varsigma = A_e/A_p = r_e^2/r_p^2 = (1-\lambda_i)^2$. Thus, the gas permeation selectivity for molecule i over j by size exclusion effect at the pore opening can be related to the molecular weight and kinetic size and the pore size as

$$\alpha^o_{i/j} \propto \left(\frac{1-\lambda_i}{1-\lambda_j}\right)^2 \cdot \frac{\sqrt{M_{w,j}}}{\sqrt{M_{w,i}}} \cdot \exp\left(-\frac{E_{a,i} - E_{a,j}}{RT}\right), \lambda_i = r_{k,i}/r_p \quad (5)$$

where $E_{a,i}$ is the energy barrier for molecule i to enter the zeolitic channel, which is presumably dependent of λ_i. It is well-known that molecules can enter zeolites even when the nominal r_k and r_p are equal (i.e., λ_i = 1) or r_k is slightly bigger than r_p (i.e., $\lambda_i > 1$). Thus, theoretically quantifying $\alpha_{i/j}$ or $\alpha^o_{i/j}$ is difficult because both the zeolitic pores and molecular size are not exactly known due to their structural flexibility. Nevertheless, relation (5) can still help understanding the size exclusion effects. Figure 13 shows the relation between $[(1-\lambda_{O2})^2/(1-\lambda_{N2})^2 \cdot (\sqrt{M_{w,N2}}/\sqrt{M_{w,O2}})]$ and d_p that is predicted for the ideal system of rigid pore opening and hard sphere molecules. Because $E_{a,O2} < E_{a,N2}$, the value of $\exp[-(E_{a,i} - E_{a,j})/RT]$ is always >1; therefore, $\alpha^o_{O2/N2} > [(1-\lambda_{O2})^2/(1-\lambda_{N2})^2 \cdot (\sqrt{M_{w,N2}}/\sqrt{M_{w,O2}})]$. Apparently, $[(1-\lambda_{O2})^2/(1-\lambda_{N2})^2 \cdot (\sqrt{M_{w,N2}}/\sqrt{M_{w,O2}})]$ and consequently $\alpha^o_{O2/N2}$ remains close to 1.0 when d_p is relatively large (e.g., d_p > 0.45 nm) and increases sharply when d_p becomes < 0.4 nm to approach $d_{k,N2}$.

The above simple calculation indicates a conservative estimate of $\alpha^o_{O2/N2} > 4.22$ for $d_p < 0.38$ nm by size-selectivity at the pore entrance, which is significantly greater than the $\alpha^o_{O2/N2}$ of the CCD modified membranes in this study. The O_2/N_2 selectivity was thus believed to be lowered primarily by gas

permeation through the intercrystalline pores where the molecular transport is mainly governed by the gaseous diffusion mechanism and selective towards N_2 [26].

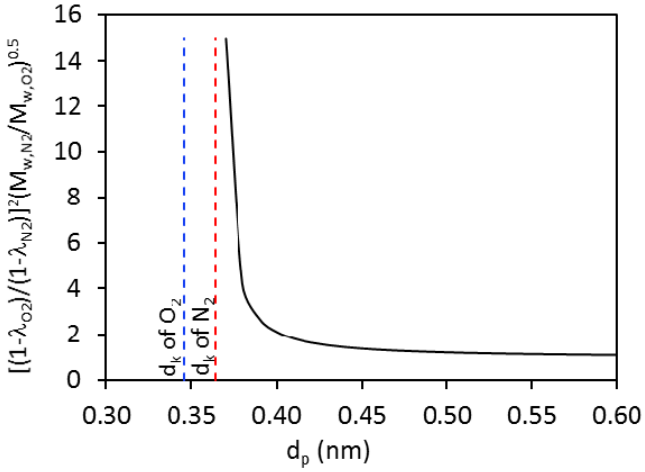

Figure 13. Dependence of $[(1-\lambda_{O2})^2/(1-\lambda_{N2})^2 \cdot (\sqrt{M_{w,N2}}/\sqrt{M_{w,O2}})]$ on d_p.

3.6. Reduction of Intercrystalline Spaces

Preliminary experiment was carried out in attempt to reduce the intercrystalline spaces and improve the O_2/N_2 separation selectivity by liquid phase deposition of silica using tetramethoxysilane (TMOS) as the precursor. This chemical liquid deposition (CLD) method was recently developed and proven very effective for filling the nonzeolitic spaces in the DDR zeolite membrane to enhance the small gas permeation selectivity [6].

An MFI-type membrane was prepared using the same precursor and the same synthesis procedure as described earlier. The membrane was however obtained by two times of hydrothermal treatment that minimized nonzeolitic pores in the membrane as evidenced by its very small $\alpha_{O2/N2}$ ($\approx$0.1) for separation of an equimolar H_2/CO_2 mixture at room temperature. The CCD modification was terminated in 4 h when the online-monitored $\alpha_{O2/N2}$ and $P_{m,H2}$ stabilized at 14 and of 1.2×10^{-7} mol/m^2·s·Pa, respectively. The CCD modified membrane was tested for O_2/N_2 separation and then treated by the CLD method for reducing the intercrystalline pores, which was similar to that reported in literature [27,28]. The CLD modification was conducted by the following procedure. First, the alumina substrate of the disc membrane was soaked with water and any liquid water was wiped off the substrate surface; second, the zeolite membrane surface was dried by sweeping with compressed air for about 10 s after the membrane disc was mounted in a permeation cell; third, the liquid TMOS was immediately filled into the cell chamber on the zeolite surface side while the chamber on the substrate side was filled with D.I. water; finally, the membrane cell was kept static at room temperature with the zeolite membrane surface facing upward for 2 h. During the finally step, TMOS hydrolysis and hydrous silica deposition took place inside the intercrystalline spaces by liquid phase counter diffusion of TMOS and water but not in the zeolitic pores because d_k of TMOS is far bigger than the zeolitic pore diameter. After the CLD process, the membrane disc was dried at 333 K for 1 day followed by further drying at 473 K for 6 h and finally calcined at 723 °C for 6 h.

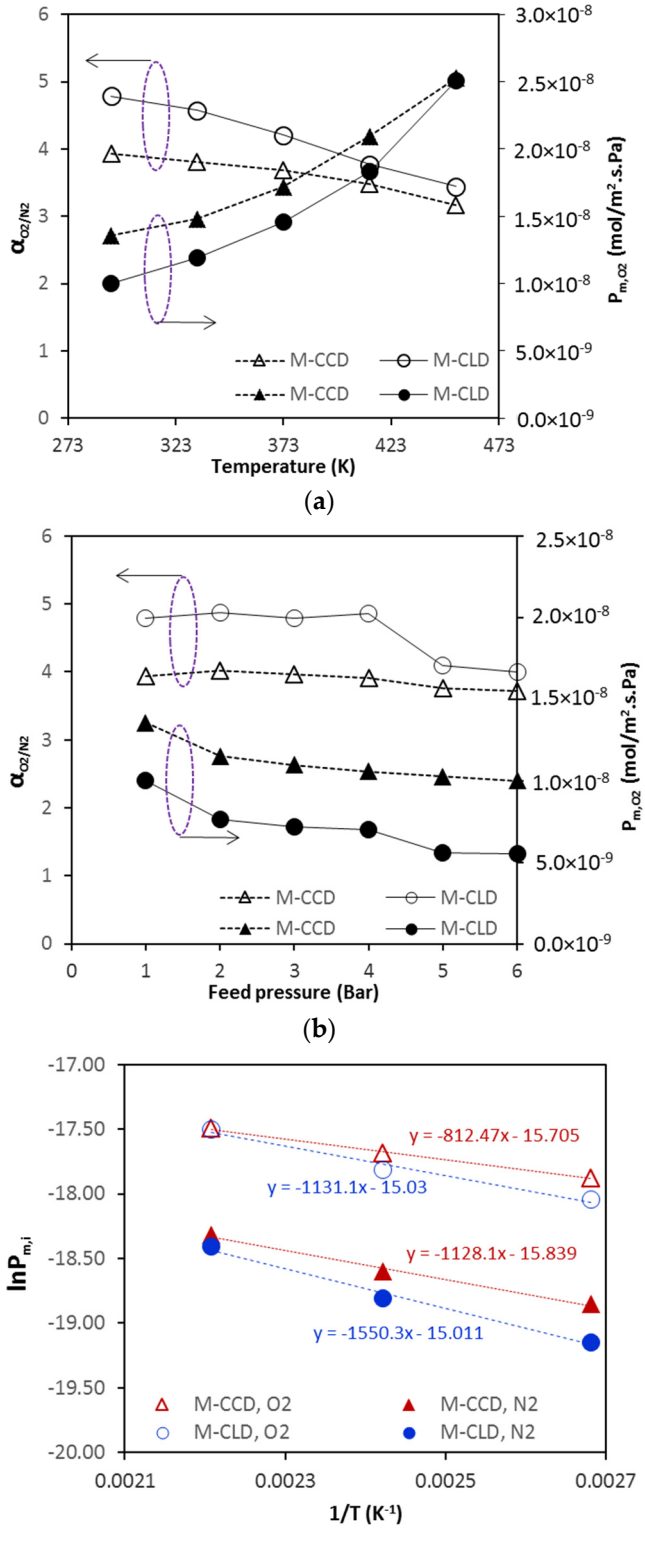

Figure 14. Results of separation of equimolar O_2/N_2 gas mixture on the CCD modified membrane before (M-CCD) and after the CLD treatment (M-CLD). (**a**) $\alpha_{O2/N2}$ and $P_{m,O2}$ as functions of temperature; (**b**) $\alpha_{O2/N2}$ and $P_{m,O2}$ as functions of feed pressure; and (**c**) Arrhenius plots of gas permeance.

The CLD modified zeolite membrane was again tested for separation of an O_2/N_2 equimolar mixture in a temperature range of 293–473 K and a feed pressure range of 1–6 bar. The O_2/N_2 separation results obtained on the CCD-modified membrane before and after the CLD treatment are presented in Figure 14. The modified membrane is named as M-CCD before the CLD treatment and named as M-CLD after CLD treatment. The temperature- and pressure-dependencies of $\alpha_{O2/N2}$ and $P_{m,O2}$ for M-CCD and M-CLD were in general consistent with those for M-M1Si and M-M2Al, both decrease moderately with increasing temperature or pressure. However, M-CCD and M-CLD exhibited significantly high $\alpha_{O2/N2}$ but much lower $P_{m,O2}$ as compared to M-M1Si and M-M2Al because the former was obtained by two time of hydrothermal crystallization that resulted in thicker membrane with less microdefects. The M-CLD had notable improvement in $\alpha_{O2/N2}$ but with large decreases in $P_{m,O2}$ as compared to M-CCD that demonstrated the effective reduction of intercrystalline spaces by the CLD modification. The best $\alpha_{O2/N2}$ on the M-CLD was nearly 5 but the $P_{m,O2}$ was only ~1.0×10^{-8} mol/m^2·s·Pa, which was less than 10% that of the M-M2Al. Figure 14c presents the Arrhenius correlations of gas permeance at relatively high temperatures ($\geq$373 K) for M-CCD and M-CLD. The $E_{d,O2}$ and $E_{d,N2}$ of M-CCD were 6.75 kJ/mol and 9.38 kJ/mol, respectively, which were very similar to the values observed in M-M2Al as expected. The $E_{d,O2}$ and $E_{d,N2}$ of M-CLD increased to 9.40 kJ/mol and 12.89 kJ/mol, respectively; both became significantly greater than the values of M-CCD that further indicated the effective reduction of gaseous diffusion through the intercrystalline spaces by the CLD modification.

4. Conclusions

The CCD modified MFI-type zeolite has been demonstrated to have O_2/N_2 permselectivity and mixture separation factor around 2. The O_2 permeance was drastically enhanced for the modified MFI zeolite membrane by forming of an alumina-containing zeolite membrane surface, which effectively limited the channel narrowing within a small thickness near the outer surface by CCD modification. The modified membrane with a ZSM-5 surface (i.e., M-M2Al) had a moderately lower $\alpha_{O2/N2}$ (~1.95) than the modified membrane M-M1Si ($\alpha_{O2/N2}$~2.25) but the former had a $P_{m,O2}$ of 1.2×10^{-7} mol/m^2·s·Pa, which was 16 times that of the M-M1Si ($P_{m,O2} = 7.24 \times 10^{-9}$ mol/m^2·s·Pa). The theoretical analysis of size exclusion effect by the reduced pore size was carried out based on a simplified system of rigid pore openings and hard sphere molecules. The results suggested that the CCD modified MFI-type zeolite membrane was expected to possess much higher O_2/N_2 selectivity than those obtained on the two CCD modified membranes. The lower-than-expected $\alpha_{O2/N2}$ on the modified membranes was attributed to the inevitably existing intercrystalline spaces, which allow the undesirable gas transport by gaseous diffusion to lower the O_2/N_2 selectivity. Preliminary investigation on CLD treatment of a CCD modified MFI-type zeolite membrane demonstrated that O_2 selectivity of the modified zeolite membrane could be further improved by reducing the nonzeolitic pores by repeated hydrothermal synthesis and the CLD repairing of intercrystalline pores. The CLD-modified membrane achieved an impressive $\alpha_{O2/N2}$ of 4.9 but with a low $P_{m,O2}$ of ~1.0×10^{-8} mol/m^2·s·Pa. To further improve the separation of small gases such as the O_2/N_2 mixture, the challenge of synthesizing high quality silicalite membranes with very small thickness and a ZSM-5 surface need to be addressed so that the membrane can achieve both high selectivity and high permeance after the CCD modification.

Acknowledgments: This research was financially supported by the U.S. Department of Energy/NETL through grant number DE-FE0026435 and the Development Service Agency of Ohio through the Ohio Coal Research and Development program (Grants # OOECDO-D-15-16 and # OOECDO-D-17-13).

Author Contributions: S. Yang and A. Arvanitis designed and performed the experiments and did main part of the data analyses; Z. Cao and X. Sun involved in the synthesis and characterization work; J. Dong directed the research, conceived the concept, and contributed to the data analyses and theoretical work.

Conflicts of Interest: The authors declare no conflict of interest.

References

1. Baker, R.W. Future directions of membrane gas separation technology. *Ind. Eng. Chem. Res.* **2002**, *41*, 1393–1411. [CrossRef]
2. Xiao, J.; Wei, J. Diffusion mechanism of hydrocarbon in zeolites-1. Theory. *Chem. Eng. Sci.* **1992**, *47*, 1123–1141. [CrossRef]
3. Tang, Z.; Nenoff, T.M.; Dong, J. Internal surface modification of MFI-type zeolite membranes for high selectivity and high flux for hydrogen. *Langmuir* **2009**, *25*, 4848–4852. [CrossRef] [PubMed]
4. Tomita, T.; Nakayama, K.; Sakai, H. Gas separation characteristics of DDR type zeolite membrane. *Micropor. Mesopor. Mater.* **2004**, *68*, 71–75. [CrossRef]
5. Van den Bergh, J.; Zhu, W.; Gascon, J.; Moulijn, J.A.; Kapteijn, F. Separation and permeation characteristics of a DD3R zeolite membrane. *J. Membr. Sci.* **2008**, *316*, 35–45. [CrossRef]
6. Yang, S.; Cao, Z.; Arvanitis, A.; Sun, X.; Xu, Z.; Dong, J. DDR-type zeolite membrane synthesis, modification and gas permeation studies. *J. Membr. Sci.* **2016**, *505*, 194–204. [CrossRef]
7. Yin, X.; Zhu, G.; Yang, W.; Li, Y.; Zhu, G.; Xu, R.; Sun, J.; Qiu, S.; Xu, R. Stainless-steel-net-supported zeolite NaA membrane with high permeance and high permselectivity for oxygen over nitrogen. *Adv. Mater.* **2005**, *17*, 2006–2010. [CrossRef]
8. Zhu, W.; Gora, L.; van den Berg, A.W.C.; Kapteijn, F.; Jansen, J.C.; Moulijn, J.A. Water vapour separation from permanent gases by a zeolite-4A membrane. *J. Membr. Sci.* **2005**, *253*, 57–66. [CrossRef]
9. Caro, J.; Albrecht, D.; Noack, M. Why is it so extremely difficult to prepare shape-selective Al-rich zeolite membranes like LTA and FAU for gas separation? *Sep. Purif. Technol.* **2009**, *66*, 143–147. [CrossRef]
10. Masuda, T.; Fukumoto, N.; Kitamura, M.; Mukai, S.R.; Hashimoto, K.; Tanaka, T.; Funabiki, T. Modification of pore size of MFI-type zeolite by catalytic cracking of silane and application to preparation of H_2-separating zeolite membrane. *Micropor. Mesopor. Mater.* **2001**, *48*, 239–245. [CrossRef]
11. Hong, M.; Falconer, J.L.; Noble, R.D. Modification of Zeolite Membranes for H_2 Separation by Catalytic Cracking of Methyldiethoxysilane. *Ind. Eng. Chem. Res.* **2005**, *44*, 4035–4041. [CrossRef]
12. Gu, X.; Tang, Z.; Dong, J. On-stream modification of MFI zeolite membranes for enhancing hydrogen separation at high temperature. *Micropor. Mesopor. Mater.* **2008**, *111*, 441–448. [CrossRef]
13. O'Connor, C.T.; Moller, K.P.; Manstein, H. The Effect of Silanization on the Catalytic and Sorption Properties of Zeolites. *CatTech* **2001**, *5*, 172–182. [CrossRef]
14. Hong, Z.; Wu, Z.; Zhang, Y.; Gu, X. Catalytic cracking deposition of Methyldiethoxysilane for modification of zeolitic pores in MFI/α-Al_2O_3 zeolite membrane with H^+ ion exchange pretreatment. *Ind. Eng. Chem. Res.* **2013**, *52*, 13113–13119. [CrossRef]
15. Wang, H.; Lin, Y.S. Synthesis and modification of ZSM-5/silicalite bilayer membrane with improved hydrogen separation performance. *J. Membr. Sci.* **2012**, *396*, 128–137. [CrossRef]
16. Dong, J.; Lin, Y.S. In situ synthesis of P-type zeolite membranes on porous alpha-alumina supports. *Ind. Eng. Chem. Res.* **1998**, *37*, 2404–2409. [CrossRef]
17. Baerlocher, C.; McCusker, L.B.; Olson, D.H. *Atlas of Zeolite Framework Types*, 6th ed.; Elsevier: Oxford, UK, 2007.
18. Dong, J.; Wegner, K.; Lin, Y.S. Synthesis of submicron silicalite membranes on porous ceramic supports. *J. Membr. Sci.* **1998**, *148*, 233–241. [CrossRef]
19. Dong, J.; Lin, Y.S.; Hu, M.Z.C.; Peascoe, R.A.; Payzant, E.A. Template-removal-associated microstructural development of porous-ceramic-supported MFI zeolite membranes. *Micropor. Mesopor. Mater.* **2000**, *34*, 241–253. [CrossRef]
20. Dunne, J.A.; Rao, M.; Sircar, S.; Gorte, R.J.; Myers, A.L. Calorimetric heats of adsorption and adsorption isotherms. 2. O_2, N_2, Ar, CO_2, CH_4, C_2H_6, and SF_6 on NaX, H-ZSM-5, and Na-ZSM-5 zeolites. *Langmuir* **1996**, *12*, 5896–5904. [CrossRef]
21. Bernal, M.P.; Bardaji, M.; Coronas, J.; Santamaria, J. Facilitated transport of O_2 through alumina-zeolite composite membranes containing a solution with a reducible metal complex. *J. Membr. Sci.* **2002**, *203*, 209–213. [CrossRef]
22. Dong, J.; Lin, Y.S.; Liu, W. Multicomponent hydrogen/hydrocarbon separation by MFI-type zeolite membranes. *AIChE J.* **2000**, *46*, 1957–1966. [CrossRef]
23. Kanezashi, M.; O'Brien-Abraham, J.; Lin, Y.S.; Suzuki, K. Gas permeation through DDR-type zeolite membranes at high temperatures. *AIChE J.* **2008**, *54*, 1478–1486. [CrossRef]

24. Babarao, R.; Jiang, J. Diffusion and separation of CO_2 and CH_4 in silicalite, C-168 schwarzite, and IRMOF-1: A comparative study from molecular dynamics simulation. *Langmuir* **2008**, *24*, 5474–5484. [CrossRef] [PubMed]
25. Gu, Y.; Hacarlioglu, P.; Oyama, S.T. Hydrothermally stable silica-alumina composite membranes for hydrogen separation. *J. Membr. Sci.* **2008**, *310*, 28–37. [CrossRef]
26. Dong, J.; Lin, Y.S.; Kanezashi, M.; Tang, Z. Microporous inorganic membranes for high temperature hydrogen purification. *J. Appl. Phys.* **2008**, *104*, 121301. [CrossRef]
27. Zhang, B.; Wang, C.; Lang, L.; Cui, R.; Liu, X. Selective defect-patching of zeolite membranes using chemical liquid deposition at organic/aqueous interfaces. *Adv. Funct. Mater.* **2008**, *18*, 3434–3443. [CrossRef]
28. Hong, Z.; Zhang, C.; Gu, X.; Jin, W.; Xu, N. A simple method for healing nonzeolitic pores of MFI membranes by hydrolysis of silanes. *J. Membr. Sci.* **2011**, *366*, 427–435. [CrossRef]